

## **Organohalide Perovskites Are Fast Ionic Conductors**

*Nuria Vicente and Germà Garcia-Belmonte\**

N. Vicente, Prof. G. Garcia-Belmonte

Institute of Advanced Materials (INAM), Universitat Jaume I, 12006 Castelló, Spain

E-mail: garciag@uji.es

Keywords: perovskites, ion conduction, batteries, impedance, lithium-ion diffusion

Fast ionic conductors constitute a family of materials exhibiting high values of the ionic conductivity while their crystal structure remains rather rigid. Perovskite-like compounds are known to be good ionic conductors with applications as solid electrolytes. In hybrid halide perovskites both intrinsic (native) and extrinsic defect migration are regarded to occur. Ion diffusivity analysis is inherently ambiguous in all-solid-state configurations because of the multicomponent environment. Here a liquid electrolyte in contact to the perovskite material forms a reservoir of  $\text{Li}^+$  that is forced to intercalate and migrate within the perovskite electrode. This approach decouples different contributions to transport in such a way that ion diffusion kinetics is easily accessible by means of impedance methods. Room-temperature chemical diffusion coefficient of lithium-ion within the perovskite lattice exhibits values as high as  $D_{\mu} \sim 10^{-7} \text{ cm}^2 \text{ s}^{-1}$ , which implies conductivities within the range of  $10^{-3} \text{ } \Omega^{-1} \text{ cm}^{-1}$  for highly lithiated electrodes. This confirms the superionic intrinsic property of organohalide perovskites from a direct and unambiguous measurement that does not rely upon simulation tools.

Fast ionic conductors (also known as superionic conductors) constitute a family of materials exhibiting high values of the ionic conductivity or diffusivity.<sup>[1, 2]</sup> Their principal feature is the ability to keep the crystal structure rather frozen while permitting the migration of ionic species. Fast ionic conductors are of particular interest for technological applications in the field of solid electrolytes for electrochemical devices such as batteries, supercapacitors, sensors, electrochromic windows, and ionic membranes for fuel cells. Typically ionic conductivity lies within the range of  $10^{-4} - 10^{-1} \Omega^{-1} \text{ cm}^{-1}$  at room temperature to consider a material as superionic conductor. Some fast ionic conductors also exhibit prominent electronic conductivity and are known as mixed ionic-electronic conductors. Many perovskite-type oxides belong to this class of materials and have well-known applications in solid-oxide fuel cells and oxygen permeation membranes.<sup>[3, 4]</sup> Even halide perovskites of the type  $\text{CsPbX}_3$  ( $\text{X}=\text{Cl}, \text{Br}$ ) are also known to be good ionic conductors.<sup>[5]</sup> Native defects in hybrid lead halide perovskite materials are known to migrate within the perovskite lattice because of the soft character of the compounds. First-principles computational studies have identified facile migration of iodine anions through a vacancy-assisted mechanism, and also long-range displacement of the organic cation, although different calculated activation energies have been reported.<sup>[6-8]</sup> These simulations observe presence in equilibrium of several ionic vacancies and interstitials ( $\text{I}^-$ ,  $\text{Br}^-$ ,  $\text{Pb}^{2+}$  and  $\text{CH}_3\text{NH}_3^+$ ) at room temperature. Also extrinsic defects as hydrogen has been studied by First-principles.<sup>[9]</sup> However, there is no clear agreement concerning the ion diffusion time scale or the dominant ionic species. Whereas some studies have reported diffusivity values of native defects in organohalide perovskites of the order of those encountered in common solid state ionic conductors,  $D \sim 10^{-12} \text{ cm}^2 \text{ s}^{-1}$ ,<sup>[7, 10, 11]</sup> other analyses give much faster ion migration coefficients  $D \sim 10^{-8} - 10^{-7} \text{ cm}^2 \text{ s}^{-1}$ .<sup>[12, 13]</sup> Despite the recognized need for knowing about the kinetics of

ion migration, the complex defect chemistry exhibited by organohalide perovskites makes it difficult discerning about specific mobile ion diffusivity.

Since determination of defect diffusivities in perovskite films is inherently complex, it is proposed here an approach that takes advantage of the intercalation and migration of extrinsic lithium ions into methylammonium lead bromide perovskite to unambiguously extract diffusivity values. Instead of working on all-solid-state configurations, a reservoir of  $\text{Li}^+$  makes part of the liquid electrolyte in contact to the perovskite material. In this configuration (**Figure 1a**)  $\text{Li}^+$  is forced to intercalate and migrate within the perovskite electrode in such a way that the ion diffusion kinetics is easily accessible by means of impedance methods. Provided the mixed conduction character of organohalide perovskites with very high electronic mobilities,<sup>[14]</sup> our approach decouples the electronic from the ionic transport thereby avoiding the intrinsic ambiguity of solid state methods. This is feasible because both electronic and ionic densities increase by the same amount upon intercalation, in such away that electronic conductivity always exceeds the ionic conductivity. It is the slowest charge carrier that determines the kinetics.

In the present work, the hybrid perovskite  $\text{CH}_3\text{NH}_3\text{PbBr}_3$  has been utilized as active material for the anode electrode of lithium-ion half-battery set-up (Figure 1a). Easy  $\text{Li}^+$  intercalation is related to the framework of corner-connected  $\text{MX}_6$  ( $\text{M} = \text{Pb}$ ,  $\text{X} = \text{Br}$ ) octahedrons with organic methylammonium cations located between them.<sup>[15]</sup> The hybrid halide perovskite behaves as a compact structure in which the dimensionality of  $\text{Li}^+$  transport is 3D similarly to that occurring for intercalation spinel compounds such as  $\text{LiMn}_2\text{O}_4$ . Moreover, perovskite electrodes allow checking ion diffusion dynamics of extrinsic defects ( $\text{Li}^+$ ) in a fully controllable way. Hence, our strategy avoids the inherent uncertainty found in analyzing native defect migration in a multicomponent environment. It is observed that room-temperature chemical diffusion coefficient of lithium-ion within the perovskite lattice exhibits

values as high as  $D_{\mu} \sim 10^{-7} \text{ cm}^2 \text{ s}^{-1}$ , which implies ionic conductivities within the range of  $10^{-3} \text{ } \Omega^{-1} \text{ cm}^{-1}$  for highly lithiated electrodes. This confirms the fast ionic conductor character of hybrid perovskite materials from a direct and unambiguous measurement that does not rely upon simulation tools.

Perovskite-based electrodes are prepared as described in the Experimental Section and recently reported.<sup>[16]</sup> XRD analysis confirms the pure perovskite crystallographic phase (Figure 1b). Electrodes comprises  $\text{CH}_3\text{NH}_3\text{PbBr}_3$  composed of 65 nm average size particles, conductive carbon black and poly(vinylidenedifluoride) binder (PVDF, Sigma-Aldrich), with a 80:10:10 weight ratio, deposited on Cu foils (Figure 1a). The use of carbon black assures a good electronic connection between Cu and the perovskite particles. The driving force for  $\text{Li}^+$  transport relates to the ion chemical potential gradient  $\Delta\mu$  that establishes the electrode potential as  $eV = -[\mu(x) - \mu_{ref}]$ , being  $e$  the positive elementary charge,  $x$  is the molar concentration in  $\text{Li}_x\text{CH}_3\text{NH}_3\text{PbBr}_3$ , and  $\mu_{ref}$  refers to the Li-metal electrode potential reference. For testing electrochemical response, perovskite-based anodes were monitored by cyclic voltammetry (see Experimental Section for details). Figure 1c shows stable signal that does not change significantly through continuous cycling.<sup>[16]</sup> It confirms a good reversibility for the electrode material. The reaction peaks related to  $\text{Li}^+$  insertion are observed at 0.49 V and 0.27 V vs.  $\text{Li}/\text{Li}^+$ , and the  $\text{Li}^+$  extraction from the matrix produces two peaks in the delithiation current at 0.65 V and 0.75 V vs.  $\text{Li}/\text{Li}^+$ . Contrary to that occurring for conducting polymer<sup>[17]</sup> or redox molecule modified electrodes,<sup>[18]</sup> in which the energy landscape of electronic states dictate the electrochemical response, perovskite-based anodes are driven by the ionic energetics. As recently reported,  $\text{CH}_3\text{NH}_3\text{PbBr}_3$  electrodes exhibit a highly reversible lithium uptake and release without severe distortion of the perovskite lattice (topotactic intercalation). Even the basic band structure remains basically unaltered for the potential window of interest.<sup>[16]</sup> As observed in Figure 1c, electrodes comprising perovskite precursors

(PbBr<sub>2</sub>) have no electrochemical activity in comparison to perovskite-based electrodes. Hence, the electrochemical set-up used here constitutes an excellent approach to investigate ion diffusion through the perovskite lattice.

Electrochemical impedance spectroscopy (EIS) analysis is performed potentiostatically at different charge states after the first cycles, for discharging (lithiation) steps of 50 mC. Galvanostatic lithiation profile of electrodes within the voltage range 1.80 V to 0.01 V vs Li/Li<sup>+</sup> during EIS measurements is shown in **Figure 2a**. See recent report on charge/discharge curves and rate capability.<sup>[16]</sup> The impedance plots in Figure 2b consist of three well-defined parts: the high-frequency semicircle related to electrode/electrolyte processes, the middle frequency diffusion pattern, and an inclined low-frequency line in response to the electrochemical charging. The impedance spectra could be modeled by means of a well-known Randles' equivalent circuit as shown in inset of Figure 2a. The equivalent circuit includes a parallel subcircuit of  $R_{ct}$  and  $C_{dl}$  that accounts for the polarization charge-transfer resistance and the double-layer capacitance associated to the electrode/electrolyte interface. At high frequencies, a rather voltage- and electrode thickness-independent arc is found with  $C_{dl} \approx 2.8 \text{ mF g}^{-1}$  ( $C_{dl} \approx 10 \text{ } \mu\text{F cm}^{-2}$ ; see Figure S1) and  $R_{ct} \approx 0.14 \text{ } \Omega \text{ g}$  ( $R_{ct} \approx 20.16 \text{ } \Omega \text{ cm}^2$ ). These trends and values allow readily connecting them to mechanisms occurring at the outer electrode/electrolyte interface. In addition, series resistance accounts for the ohmic resistance  $R_s \approx 0.04 \text{ } \Omega \text{ g}$  ( $R_s \approx 5.6 \text{ } \Omega \text{ cm}^2$ ).

The intermediate- and low-frequency impedance response points to a diffusive-capacitive behavior that depends on the voltage (charge) state. This performance informs on the electrode ability of varying its capacity because of the intercalation of Li<sup>+</sup> inside perovskite structure. By examining this behavior, it is possible to know how fast ions can be inserted into or withdrawn (extracted) from a rather stable host crystal lattice. The impedance model used here corresponds to the classical spatially restricted diffusion element, which exhibits the so-

called anomalous diffusion response,  $Z_D$  in the inset of Figure 2a.<sup>[19]</sup> This scheme assumes large enough electronic conductivity so as to render  $\text{Li}^+$  diffusion as determining parameter of the charging process. This is expected to be the case provided the high electronic mobility reported for solar perovskite materials.<sup>[14]</sup> Diffusion impedances undergo a pattern change at a certain characteristic frequency  $\omega_d$  at which a transition between a Warburg- to a capacitive-like behavior is observed.<sup>[20, 21]</sup> The frequency  $\omega_d$  is located near the elbow of the impedance plot, as marked in Figure 2b, and relates to the chemical diffusion coefficient  $D_\mu$  as

$$\omega_d = \frac{D_\mu}{L^2} \quad (1)$$

Here  $L$  accounts for the thickness of the electrode. The finite-length diffusion element is given by

$$Z_D = R_d (i\omega / \omega_d)^{-\gamma/2} \coth \left[ (i\omega / \omega_d)^{-\gamma/2} \right] \quad (2)$$

being  $\omega$  the angular frequency, and  $i = \sqrt{-1}$ .  $R_d$  is the resistance associated with the ionic diffusion, and  $\gamma$  relates to the deviation from the ideal spatially restricted diffusion impedance ( $\gamma=1$ ). The anomalous diffusion mechanism ( $\gamma < 1$ ) is expected to occur in a multiphase matrix.<sup>[22]</sup> Models based on spatially-restricted ion diffusion were proposed to account for intermediate-frequency distortions relating on a distribution of diffusion lengths,<sup>[23]</sup> or electronic transport limitations.<sup>[24]</sup> Diffusion of ions gives rise to distinctive impedance patterns characterized by Warburg-like responses as  $Z \propto (i\omega)^{-\gamma/2}$  at intermediate frequencies. At lower frequencies the electrode charging is manifested in the capacitive response of the impedance through the chemical capacitance  $C_\mu = e^2 N dx / d\mu$  element, being  $N$  the total density of intercalation ion sites in the perovskite lattice. It is related to the characteristic frequency as

$$\omega_d = \frac{1}{R_d C_\mu} \quad (3)$$

By fitting the equivalent circuit in the inset of Figure 2a to the impedance data in Figure 2b for different voltage stages during discharge process, it is found that the diffusion resistance decreases with voltage, from 0.18  $\Omega$  g at 1.20 V down to 0.08  $\Omega$  g at 0.30 V. It is also checked for consistency that the chemical capacitance extracted from impedance and that derived from cyclic voltammetry as  $C_\mu = -dQ/dV$  yields similar values (Figure 2c), with a voltage shift in the peak position related to kinetic limitations in the case of large-amplitude, out-of-equilibrium techniques as cyclic voltammetry at usual scan rates.

Some caution words are in order here about the applicability of the previously outlined diffusion model. The extraction of the chemical diffusion coefficient  $D_\mu$  using Equation 1 relies on a proper determination of the diffusion length that, in certain experimental conditions, does not coincide with the electrode thickness  $L$ . If the electrolyte penetrates the electrode and wets the active particles the effective diffusion length in the solid-state may be significantly reduced  $L_{\text{eff}} \ll L$ , giving rise to large overestimations in  $D_\mu$ . The so-called porous impedance model allows addressing these last cases.<sup>[23-25]</sup> Hence, it is a matter of experimental check to discern if  $L_{\text{eff}} \approx L$ , in such a way that the finite-length diffusion mechanism in Equation 2 can be exploited to determine  $D_\mu$ . Here electrodes with different thickness, by varying the weight of the active material, have been tested by impedance.

As the perovskite lithiation progresses, specific capacity values as high as 400 mA h g<sup>-1</sup> are reached (Figure 2a), which implies a Li-ion concentration as high as 10<sup>21</sup> cm<sup>-3</sup>, given perovskite densities approximately equal to 4.16 g cm<sup>-3</sup>. The host matrix becomes fully lithiated at potentials below 0.5 V, as discussed very recently.<sup>[16]</sup> It is worth determining the chemical diffusion coefficient in Equation 1, where the diffusion characteristic frequency is extracted from long-range Li<sup>+</sup> displacements corresponding to the thickness of the electrode.

The variation of the diffusion characteristic frequency  $\omega_d$  with voltage is shown in **Figure 3a**. One can observe that  $\omega_d$  appears to be rather voltage-independent but exhibits a clear correlation with the electrode thickness in agreement with Equation 1. A close examination of the average values of  $\omega_d$  as a function of  $L$  allows verifying the validity of our approach (Figure 3b). Here it has been checked that fitting the expression  $\omega_d = D_\mu L^{-n}$  yields a value for the thickness coefficient equaling  $n = 2.8 \pm 0.6$ . This agrees with the thickness dependence predicted by Equation 1 as  $n \approx 2$  within the experimental error. This observation allows extracting  $D_\mu = (2.8 \pm 1.0) \times 10^{-7} \text{ cm}^2 \text{ s}^{-1}$  given the strong correlation between  $\omega_d$  and the electrode thickness. An additional point reinforcing that  $L_{\text{eff}} \approx L$  is the electrode thickness-independent trend exhibited by the double-layer capacitance. As shown in Figure S1,  $C_{\text{dl}}$  is always situated around typical values in the order of  $\mu\text{F cm}^{-2}$ , not correlated with  $L$  at all. This is in contradiction with that derived from the porous electrode model in which the electrolyte/electrode interface is extended within the matrix producing double-layer capacitances largely exceeding  $\mu\text{F cm}^{-2}$  values.<sup>[26]</sup> Moreover, one would expect strong correlations between  $C_{\text{dl}}$  and the electrode thickness for the porous electrode model. These trends have neither been observed in our samples.

Diffusivity attains rather voltage-independent values in the range of  $D_\mu \sim 10^{-7} \text{ cm}^2 \text{ s}^{-1}$ . This high lithium diffusivity corresponds to conductivities within the range of  $10^{-3} \Omega^{-1} \text{ cm}^{-1}$  for highly lithiated electrodes. It is checked here that the procedure to determine the chemical diffusion coefficient is consistent with the electrode thickness variation. This fact allows us to discard relating  $\omega_d$  to the perovskite particle size (65 nm) and verifies the proposed diffusion model in Equation 2 in which  $L$  equals the thickness of the host matrix.

To sum up, our findings unambiguously show that lead halide perovskites can be regarded as fast ionic conductors with large diffusion coefficients. The approach followed here, using an electrolyte/electrode contact, allows decoupling electronic from ionic transport. This avoids the inherent ambiguity of all-solid-state experimental techniques. Room-temperature chemical diffusion coefficient of  $\text{Li}^+$  within the perovskite lattice exhibits values as high as  $D_{\mu} \sim 10^{-7} \text{ cm}^2 \text{ s}^{-1}$ , which implies conductivities within the range of  $10^{-3} \Omega^{-1} \text{ cm}^{-1}$  for highly lithiated electrodes. The proved superionic intrinsic property of organohalide perovskites opens new room for devising applications and devices in which fast ionic migration is an essential requirement.

## Experimental Section

Perovskite material were synthesized by slow evaporation of N, N-dimethylformamide (DMF, Sigma-Aldrich) in a solution containing stoichiometric amounts of lead bromide ( $\text{PbBr}_2$ , TCI) and methylammonium bromide ( $\text{CH}_3\text{NH}_3\text{Br}$ , >98% TCI) 1M in DMF, as recently reported.<sup>[16]</sup> Solid precipitated becomes orange at the end of the reaction. Bruker AXS-D4 Endeavor Advance X-ray diffractometer using  $\text{Cu K}\alpha$ , wavelength  $\lambda=1.5406 \text{ \AA}$ , is employed in XRD to confirm the pure perovskite crystallographic structure.

The working anode electrode (Figure 1a) was prepared by mixing  $\text{CH}_3\text{NH}_3\text{PbBr}_3$  composed of 65 nm average size particles, conductive carbon black and poly(vinylidenedifluoride) binder (PVDF, Sigma-Aldrich) with a 80:10:10 weight ratio, and N-methyl-2-pyrrolidone (NMP) as solvent.<sup>[16]</sup> Also the blank electrode comprising  $\text{PbBr}_2$  contains the same weight ratio (80:10:10). The slurry was coated on a copper foil by Dr. Blade and dried at  $100^\circ\text{C}$  overnight. Working electrodes for electrochemical analysis were made up of composite material slices with a diameter of 10 mm using Swagelok-type cells. Li metal foil was used as the counter and reference electrode (Figure 1a), and an electrolyte-soaked, microporous monolayer membrane (Celgard 2500) is employed as separator. The electrolyte is 1M of

hexafluorophosphate lithium salt ( $\text{LiPF}_6$ , Sigma-Aldrich) dissolved in ethylene carbonate, ethyl-methyl carbonate and dimethyl carbonate (EC:EMC:DMC, Sigma-Aldrich) with 1:1:1 v/v. Cell assembly was carried out in an  $\text{N}_2$  filled glovebox. For electrochemical characterization, a PGSTAT-30 potentiostat from AUTOLAB equipped with an impedance module was employed. Cyclic voltammetry (CV) was performed in the voltage range from 0.01 to 2.00V with a rate of  $5 \text{ mV s}^{-1}$ . After the first cycle, in the second discharge electrochemical impedance (EIS) test was carried out potentiostatically every 50 mC of discharge (Figure 2a), with an amplitude perturbation of 10 mV in the frequency range of 1 MHz to 10 mHz. The approximation to the different measuring voltages was galvanostatically controlled at  $50 \text{ mA g}^{-1}$  to assure the quasi-equilibrium state of the electrode. All the data are normalized to the load  $\text{CH}_3\text{NH}_3\text{PbBr}_3$  mass.

### **Supporting Information**

Supporting Information is available from the Wiley Online Library or from the author.

### **Acknowledgements**

We thank financial support by Generalitat Valenciana under Prometeo Project (PROMETEO/2014/020), and Ministerio de Economía y Competitividad (MINECO) of Spain under Project (MAT2016-76892-C3-1-R). N.V. acknowledges University Jaume I through FPI Fellowship Program (PREDOC/2015/54) and Project (UJI-B2016-35). SCIC from Universitat Jaume I is also acknowledged. The authors acknowledge Celgard for supplying separator membranes.

Received: ((will be filled in by the editorial staff))

Revised: ((will be filled in by the editorial staff))

Published online: ((will be filled in by the editorial staff))

### **References**

- [1] H. L. Tuller, P. K. Moon, *Materials Science and Engineering: B* 1988, 1, 171.
- [2] S. Adams, J. Swenson, *Phys. Rev. Lett.* 2000, 84, 4144.
- [3] M. Li, M. J. Pietrowski, R. A. De Souza, H. Zhang, I. M. Reaney, S. N. Cook, J. A. Kilner, D. C. Sinclair, *Nat. Mater.* 2014, 13, 31.
- [4] H. Hayashi, H. Inaba, M. Matsuyama, N. G. Lan, DokiyaM. , H. Tagawa, *Solid State Ionics* 1999, 122, 1.
- [5] J. Mizusaki, K. Arai, K. Fueki, *Solid State Ionics* 1983, 11, 203.
- [6] J. M. Azpiroz, E. Mosconi, J. Bisquert, F. De Angelis, *Energy Environ. Sci.* 2015, 8, 2118.
- [7] C. Eames, J. M. Frost, P. R. F. Barnes, B. C. O'Regan, A. Walsh, M. S. Islam, *Nat. Commun.* 2015, 6, 7497.
- [8] J. Haruyama, K. Sodeyama, L. Han, Y. Tateyama, *J. Am. Chem. Soc.* 2015, 137, 10048–10051.
- [9] D. A. Egger, L. Kronik, A. M. Rappe, *Angew. Chem. Int. Ed.* 2015, 54, 12437
- [10] M. Bag, L. A. Renna, R. Y. Adhikari, S. Karak, F. Liu, P. M. Lahti, T. P. Russell, M. T. Tuominen, D. Venkataraman, *J. Am. Chem. Soc.* 2015, 137, 13130.
- [11] G. Richardson, S. E. J. O'Kane, Niemann Ralf G. , T. A. Peltola, J. M. Foster, P. J. Cameron, A. B. Walker, *Energy Environ. Sci.* 2016, 9, 1476.
- [12] T.-Y. Yang, G. Gregori, N. Pellet, M. Grätzel, J. Maier, *Angew. Chem. Int. Ed.* 2015, 127, 8016
- [13] O. Almora, A. Guerrero, G. Garcia-Belmonte, *Appl. Phys. Lett.* 2016, 108, 043903.
- [14] S. D. Stranks, G. E. Eperon, G. Grancini, C. Menelaou, M. J. P. Alcocer, T. Leijtens, L. M. Herz, A. Petrozza, H. J. Snaith, *Science* 2013, 342, 341.
- [15] H.-R. Xia, W.-T. Sun, L.-M. Peng, *Chem. Comm.* 2015, 51, 13787.
- [16] N. Vicente, G. Garcia-Belmonte, *J. Phys. Chem. Lett.* 2017, 8, 1371–1374.
- [17] J. Bisquert, G. Garcia-Belmonte, J. García-Cañadas, *J. Chem. Phys.* 2004, 120, 6726.
- [18] D. A. Miranda, P. R. Bueno, *Phys. Chem. Chem. Phys.* 2016, 18, 25984.
- [19] J. Bisquert, A. Compte, *J. Electroanal. Chem.* 2001, 499, 112.
- [20] G. Garcia-Belmonte, Z. Pomerantz, J. Bisquert, J.-P. Lellouche, A. Zaban, *Electrochim. Acta* 2004, 49, 3413.
- [21] J. García-Cañadas, F. Fabregat-Santiago, I. Porqueras, C. Person, J. Bisquert, G. Garcia-Belmonte, *Solid State Ionics* 2004, 175, 521.
- [22] J. Bisquert, G. Garcia-Belmonte, A. Pitarch, *ChemPhysChem* 2003, 4, 287.
- [23] M. D. Levi, D. Aurbach, *J. Phys. Chem. B* 2004, 108, 11693.
- [24] J. P. Meyers, M. Doyle, R. M. Darling, J. Newman, *J. Electrochem. Soc.* 2000, 147, 2930.
- [25] J. Bisquert, G. Garcia-Belmonte, F. Fabregat-Santiago, A. Compte, *Electrochem. Commun.* 1999, 1, 429.
- [26] M. Haro, N. Vicente, G. Garcia-Belmonte, *Adv. Mater. Interfaces* 2015, 2, 1500369.

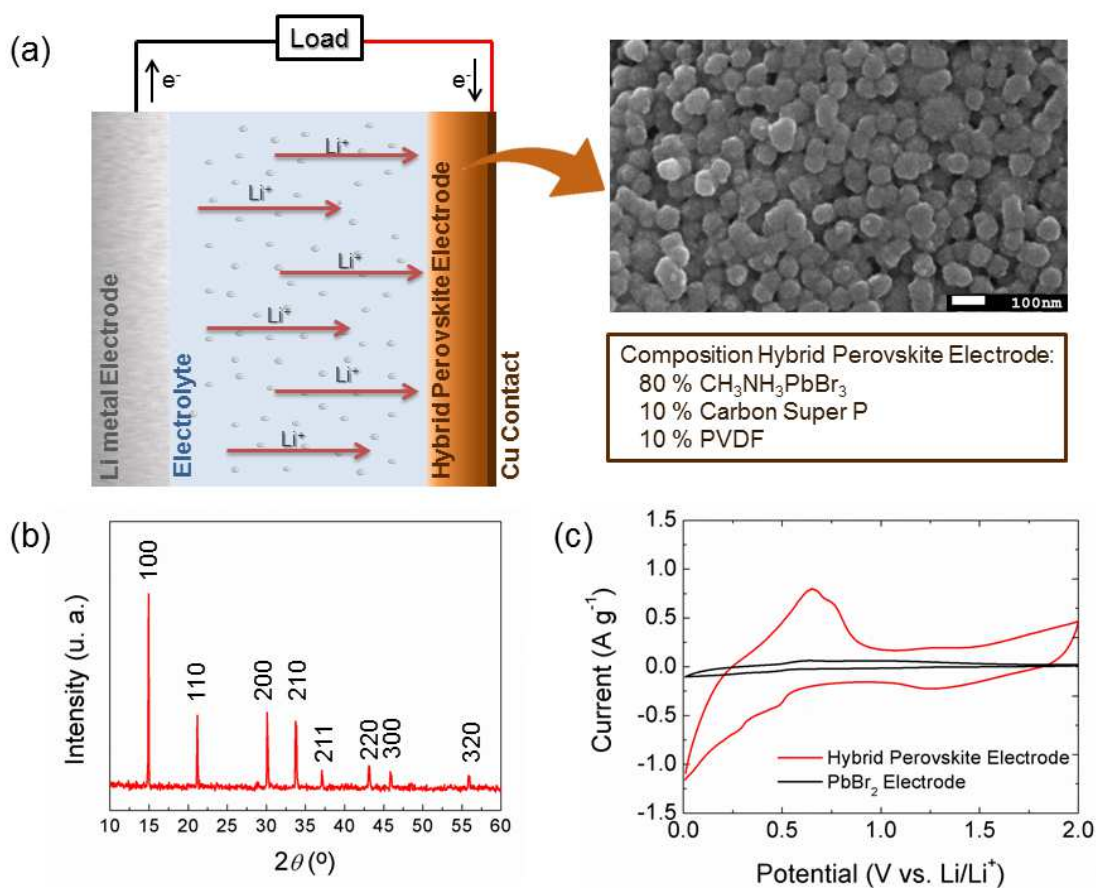


**Figure 1.** (a) Schema of half-battery set-up indicating the composition of the hybrid perovskite electrode deposited on a copper contact. SEM image showing the compact structure formed by  $CH_3NH_3PbBr_3$  particles. (b) X-ray diffraction patterns of  $CH_3NH_3PbBr_3$ . The vertical peaks correspond to the  $CH_3NH_3PbBr_3$  cubic phase signals. (c) Stable cyclic voltammetry of  $CH_3NH_3PbBr_3$  electrodes after the first four cycles, compared to the electrochemical activity of  $PbBr_2$  electrodes.

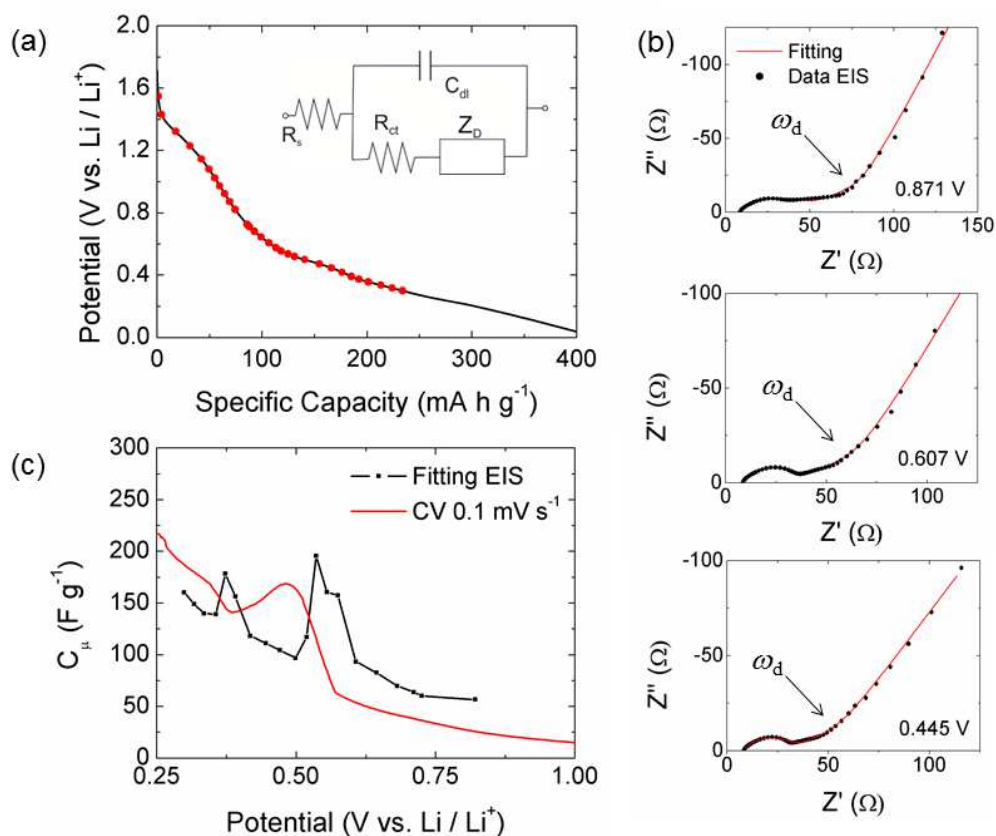


**Figure 2.** Electrochemical impedance analysis. (a) Selected potentials and charge state of the electrode lithiation process for in-situ EIS analysis during the discharge process. Inset: Randles' equivalent circuit used in the EIS fitting. (b) Impedance spectroscopy response of CH<sub>3</sub>NH<sub>3</sub>PbBr<sub>3</sub> anodes at different steady-state voltages as indicated. Solid line corresponds to fits using the equivalent circuit. The diffusion response frequency  $\omega_d$  is marked. (c)  $C_\mu$  calculated from different data: EIS and cyclic voltammetry plotted vs. potential during discharge process.

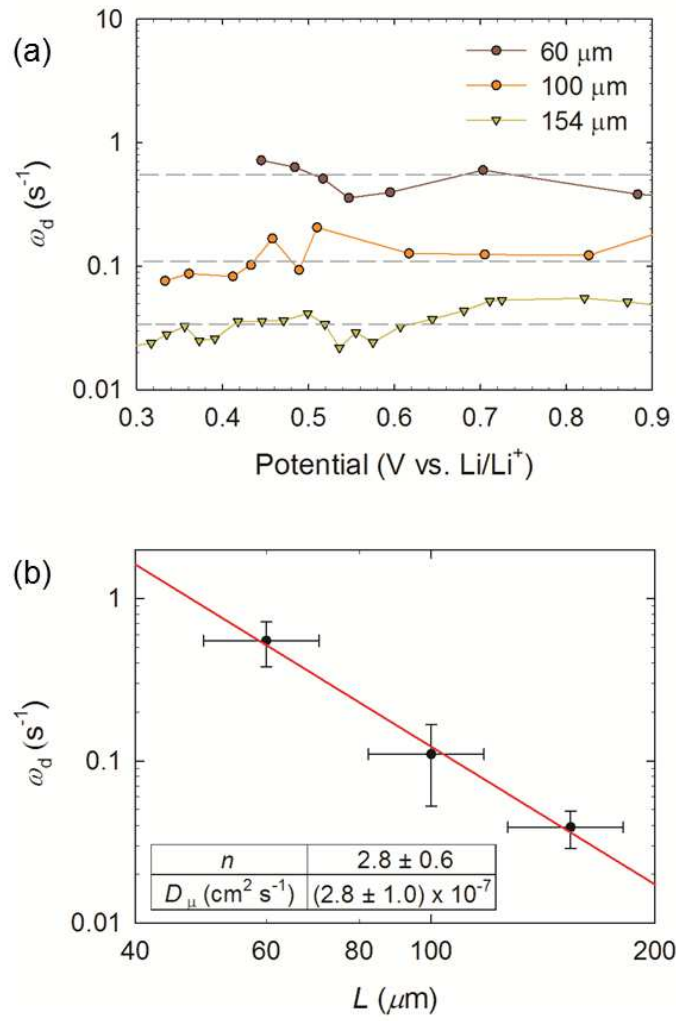


**Figure 3.** (a) Variation of the diffusion characteristic frequency  $\omega_d$  as a function of the battery voltage for three different electrode thicknesses. Dashed lines signals average frequency values. (b) Dependence of the diffusion characteristic frequency with electrode thickness. The used fitting function  $\omega_d = D_\mu L^{-n}$  provides values for  $D_\mu = (2.8 \pm 1.0) \times 10^{-7} \text{ cm}^2 \text{ s}^{-1}$ , and thickness coefficient  $n = 2.8 \pm 0.6$ , considering the experimental error.

**From impedance measurements, it is confirmed the superionic intrinsic property of organohalide perovskites.** Chemical diffusion coefficient of lithium ions is determined to be as high as  $10^{-7} \text{ cm}^2 \text{ s}^{-1}$ . The fast ionic character opens new room for devising applications and devices in which fast ionic migration is an essential requirement.

**Perovskites**

**N. Vicente, G. Garcia-Belmonte\***

**Organohalide Perovskites Are Fast Ionic Conductors**

## Supporting Information

### Organohalide Perovskites Are Fast Ionic Conductors

*Nuria Vicente and Germà Garcia-Belmonte\**

*Driven mechanism for ion intercalation.* Usually intercalation compounds operate by incorporating ionic species,  $\text{Li}^+$  most commonly, from the electrolyte. The well-known approach identifies the driving force for ion motion to the gradient in the ion chemical potential. This means that the measured potential relates to the imbalance in the ion chemical potential respect to the reference electrode (Li-metal in our case). The modification of composition in  $\text{Li}_x\text{CH}_3\text{NH}_3\text{PbBr}_3$  electrodes determines the chemical potential variation  $\mu(x)$ , with respect to Li/Li<sup>+</sup> potential  $\mu_{ref}$ . Therefore the working electrode potential is  $eV = -[\mu(x) - \mu_{ref}]$  being  $e$  the positive elementary charge. This last expression corresponds to the steady-state situation in which the Li<sup>+</sup> profile inside the electrode is considered to be position-independent. This picture assumes important points concerning the electronic charge: 1) either the chemical potential is mainly determined by the incoming ions or the electronic contribution to the chemical potential does not vary dramatically with composition. This point is fulfilled as the potential range for Li<sup>+</sup> intercalation (0.5 V vs. Li/Li<sup>+</sup>) situates more than 1.5 eV above the perovskite conduction band. 2) The electrical field is largely shielded. 3) Electronic mobility largely exceeds ionic mobility. The measured chemical capacitance  $C_\mu = e^2 N dx / d\mu$  can be determined as the inverse derivative of the equilibrium voltage–composition curve, or from the electrochemical impedance analysis because it uses a small-amplitude modulation to probe diffusion-capacitive processes.

*Decoupling ionic from electronic mobility.* Upon intercalation both electronic and ionic densities increase in the perovskite because the Cu foil and carbon used assures a good electronic contact between the active material and the external circuit. Both types of charges (electronic and ionic) participate in the intercalation kinetic process, but the largely superior electronic mobility assures that the overall mechanism is governed by the slowest charge (ions). It is known that the electronic diffusivity (electrons and holes) is  $D_e > 10^{-2} \text{ cm}^2 \text{ s}^{-1}$  (ref. 14). This assures fulfilling the condition  $D_e \gg D_i$ . This fact allows decoupling ionic from electronic mobility. Because the same amount of ionic (Li<sup>+</sup>) and electronic charge ( $e^-$ ) is inserted upon intercalation, electronic conductivity should always exceeds ionic one. This fact entails that electrons rapidly equilibrate and shield the electrical field while the ion transport effectively governs the kinetics of electrode charging to reach a given potential.

*Double-layer capacitance.* The variation of double-layer capacitance with voltage for several layer thickness values allows confirming the outlined ion diffusion model.

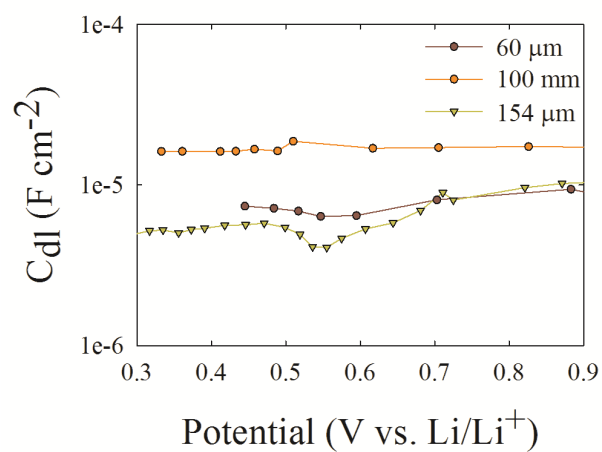


**Figure S1.** Example of variation of the double-layer capacitance as a function of the battery potential for different electrode thicknesses. As observed there is no correlation between both parameters.  $C_{dl}$  is always situated around typical values in the order of  $10 \mu\text{F cm}^{-2}$ .